THE JOURNAL OF BIOLOGICAL CHEMISTRY VOL. 289, NO. 46, pp. 32243–32252, November 14, 2014

The Isomerization of Δ^5-Androstene-3,17-dione by the Human Glutathione Transferase A3-3 Proceeds via a Conjugated Heteroannular Diene Intermediate*

Received for publication, July 31, 2014, and in revised form, September 22, 2014 Published, JBC Papers in Press, September 23, 2014, DOI 10.1074/jbc.M114.601609

Jonathan L. Daka, Ikechukwu Achilonu, and Heini W. Dirr[1]

From the Protein Structure-Function Research Unit, School of Molecular and Cell Biology, University of the Witwatersrand, Johannesburg 2050, South Africa

Background: Isomerization reactions are important biochemical transformations required to support life, but the enzymatic pathways are not fully understood.
Results: We propose a mechanism for the isomerization of androst-5-enes by glutathione transferase A3-3.
Conclusion: The glutathione transferase-catalyzed isomerization of androst-5-enes proceeds via an enforced concerted mechanism.
Significance: An understanding of the mechanism allows further insight into proton abstraction reactions in biological systems.

The seemingly simple proton abstraction reactions underpin many chemical transformations, including isomerization reactions, and are thus of immense biological significance. Despite the energetic cost, enzyme-catalyzed proton abstraction reactions show remarkable rate enhancements. The pathways leading to these accelerated rates are numerous and on occasion partly enigmatic. The isomerization of the steroid Δ^5-androstene-3,17-dione by the glutathione transferase A3-3 in mammals was investigated to gain insight into the mechanism. Particular emphasis was placed on the nature of the transition state, the intermediate suspected of aiding this process, and the hydrogen bonds postulated to be the stabilizing forces of these transient species. The UV-visible detection of the intermediate places this species in the catalytic pathway, whereas fluorescence spectroscopy is used to obtain the binding constant of the analog intermediate, equilenin. Solvent isotope exchange reveals that proton abstraction from the substrate to form the intermediate is rate-limiting. Analysis of the data in terms of the Marcus formalism indicates that the human glutathione transferase A3-3 lowers the intrinsic kinetic barrier by 3 kcal/mol. The results lead to the conclusion that this reaction proceeds through an enforced concerted mechanism in which the barrier to product formation is kinetically insignificant.

A natural consequence of the evolution of species in response to their environmental pressures has been the refinement and optimization of biological macromolecules, thus improving the functioning and adaptability of the entire organism. Enzymes are one such group of macromolecules that have been optimized to allow a more efficient flow of energy and material through a system. They display greater effectiveness than simple organic catalysts and have been the subject of much fascination because of their remarkable catalytic prowess.

In aerobic organisms, the deleterious effect of xenobiotic compounds, both of endogeneous and exogenous origin, is prevented by a superfamily of soluble dimeric proteins known as the glutathione transferases (EC 2.5.1.18) (1, 2). The detoxification reaction involves the conjugation of the toxicant with the tripeptide co-substrate glutathione (GSH), where the ionized thiol group of GSH attacks the electrophilic center of the compound. Although the soluble glutathione transferases have been grouped in different classes (alpha, pi, mu, theta, sigma, zeta, and omega), they retain a common fold, with each subunit possessing a conserved thioredoxin-like domain with a GSH binding site (G-site) and a less conserved all-α-helical hydrophobic site (H-site) for the binding of diverse nonpolar electrophiles (3). In 1976 Benson and Talalay (4) showed that a major GSH-dependent enzyme displays high isomerase activity with 3-ketosteroids, and 25 years later Johansson and Mannervik (5) identified the human glutathione transferase A3-3 (hGST A3-3) as displaying the highest isomerase activity over other members of the same class because of amino acid variations in the H-site.

The production of steroid hormones such as testosterone and progesterone from cholesterol proceeds via a complex series of oxidation and isomerization reactions (6). A critical step in this biosynthetic pathway is the isomerization of the β,γ double bond of Δ^5-androstene-3,17-dione (Δ^5-AD)[2] to the α,β isomer Δ^4-androstene-3,17-dione (Δ^4-AD); a labile hydrogen from carbon 4 adjacent to the carbonyl functional group of Δ^5-AD, is abstracted and transferred to carbon 6. In bacteria this conversion is catalyzed by ketosteroid isomerase (KSI) (7), whereas in mammalian tissue, hGST A3-3 and KSI have been shown to perform a similar task, with GSH acting as a cofactor

* This work was supported by the University of the Witwatersrand, Grants 60810, 65510, and 68898 from the South African National Research Foundation, and Grant 64788 from the South African Research Chairs Initiative of the Dept. of Science and Technology and National Research Foundation.
[1] To whom correspondence should be addressed: Protein Structure-Function Research Unit, School of Molecular and Cell Biology, University of the Witwatersrand, Johannesburg 2050, South Africa. Tel.: 27-11-717-6352; E-mail: heinrich.dirr@wits.ac.za.

[2] The abbreviations used are: Δ^5-AD, Δ^5-androstene-3,17-dione; Δ^4-AD, Δ^4-androstene-3,17-dione; KSI, ketosteroid isomerase; hGST, human glutathione *S*-transferase.

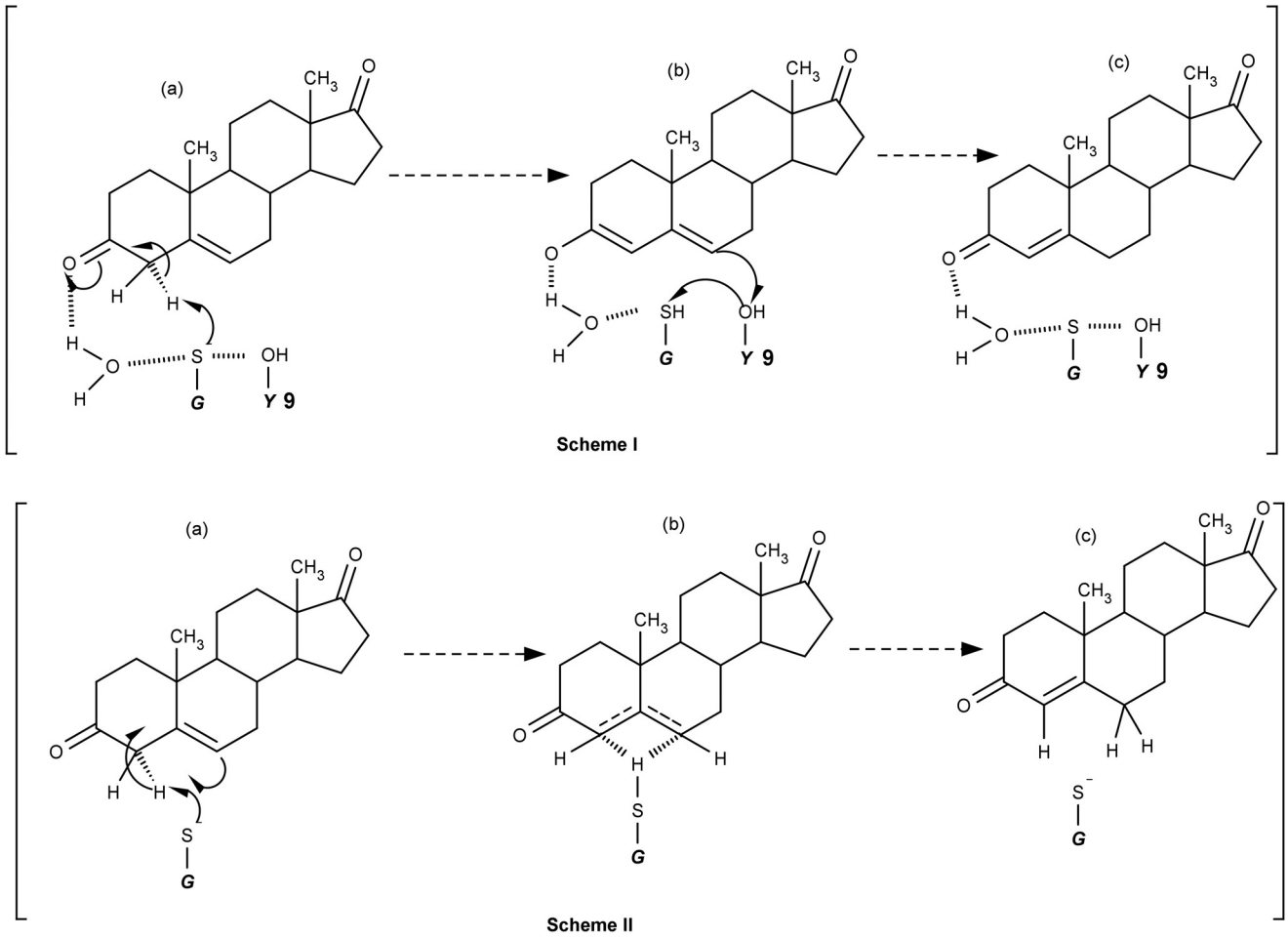

FIGURE 1. **Proposed reaction mechanisms for Δ^5-AD isomerization by hGST A3-3.** In **Scheme I**, adapted from Gu *et al.* (10), GSH abstracts the carbon 4 proton, and a water molecule acts as a hydrogen bond donor, stabilizing the negative charge on the dienolate intermediates (*a* and *b panels*). The keto form is regenerated by the transfer of negative charge via a conjugation system of π bonds with Tyr-9 acting as a proton shuttle (*c*). In **Scheme II**, adapted from Tars *et al.* (11), GSH abstracts a proton from carbon 4 while simultaneously transferring it to carbon 6. The keto group at carbon 3 is unaffected, and the reaction proceeds without the formation of the dienolate intermediate via a concerted single step mechanism.

in the hGST A3-3-catalyzed pathway but as an activator in the KSI-mediated reaction (8). Although the bacterial KSI-catalyzed conversion of Δ^5-AD has been elucidated (9), both the hGST A3-3 and mammalian KSI-catalyzed reactions remain enigmatic.

There has been much contention over the GST A3-3 catalytic conversion of Δ^5-AD to Δ^4-AD. Ji and co-workers (10) have proposed a mechanism, shown in Fig. 1, **Scheme I**, that proceeds by a stepwise pathway via the formation of a dienolate intermediate, stabilized by electron delocalization through a conjugate system of vacant *p*-orbitals along an O-C3-C4-C5-C6 pathway. It is thought that electron delocalization alone is insufficient to explain the observed catalytic rates, and a water molecule that would act as a hydrogen bond donor to the carbonyl oxygen to further stabilize the dienolate intermediate has been proposed. Structural data based on the crystal structure of a ternary complex of hGST A3-3, GSH, and the product Δ^4-AD provide no evidence of such a stabilizing water molecule, prompting Mannervik and co-workers (11) to suggest that both the bond-breaking process at carbon 4 and the bond-making process at carbon 6 is concerted and is devoid of a stable dienolate intermediate, as shown in Fig. 1, **Scheme II**. The implication is that the carbonyl oxygen plays no role in the stabilization process and electron delocalization proceeds directly from carbon 3 to carbon 6 in concert with proton transfer to carbon 6.

We sought to investigate the two proposed mechanisms in order to establish the most plausible reaction pathway. We hypothesized that if the model proposed by Mannervik and co-workers (11) is correct, there should be neither evidence of intermediate formation nor the presence of an existing water molecule at carbon 3. Furthermore we obtained the dissociation constant (K_D) for the analog intermediate, equilenin, and used this value to approximate the relative stabilities of the bound substrate and the proposed intermediate. This information, together with the pK_a values of both the free and the enzyme-bound GSH, was used to explain how the hGST A3-3 enhances the rate of proton abstraction reactions in steroidogenesis, where the Marcus formalism (12) is employed. We have further provided a molecular mechanism consistent with these results that fully explains the observed rate enhancements, with particular focus on the nature of the intermediate.

EXPERIMENTAL PROCEDURES

Materials—GSH, equilenin, 19-nortestosterone, D_2O, and K_2DPO_4 were obtained from Sigma-Aldrich. The steroid Δ^5-androstene-3,17-dione was obtained from Steraloids Inc. (Newport, RI). All other reagents were of analytical grade.

Heterologous Protein Expression and Purification—High level expression of the wild-type hGST A3-3 was based on the pET11a vector (GenScript, Inc.) in BL21(DE3) pLysS *Escherichia coli* cells. The cells were grown in 2× TY (1.6% (w/v) tryptone, 1% (w/v) yeast extract, 0.5% (w/v) NaCl) at 37 °C to an A_{600} of 0.4. A final concentration of 1 mM isopropyl-β-D-thiogalactoside was used to induce protein expression. After 4 h of growth, the cells were harvested and lysed by ultrasonication. Protein purification was by immobilized metal affinity chromatography using nickel-Sepharose (Amersham Biosciences) eluted with 20 mM Tris buffer containing 0.5 M imadazole at pH 7.4. An additional purification step using benzamidine-Sepharose produced thrombin-free pure protein. The purity was determined using SDS-polyacrylamide gel electrophoresis, and the protein was dialyzed against 20 mM sodium phosphate buffer, pH 8, containing 1 mM EDTA and 0.02% sodium azide. The concentration of the dimer was determined at 280 nm using the protein subunit molar extinction coefficient of 23,900 M^{-1} cm^{-1} (5).

Determination of the pK_a of the Thiol Group of Free and Enzyme-bound GSH—The spectrum of free GSH in solution was obtained at different pH values, and the ionization of the thiol group was monitored by measuring the absorbance of the thiolate at 239 nm. The spectrum of GSH bound to hGST A3-3 was obtained within the pH range of 5.2 to 9.3 using 0.1 M mono-, di-, and trisodium phosphate to cover the pH range and was corrected for both free GSH by subtracting the spectrum of free GSH within this pH range and free enzyme at the storage buffer pH of 7.4 from the enzyme-bound spectrum. The enzyme concentration was 9 μM, and the GSH concentration was kept at 250 μM.

Fluorescence Measurements with Equilenin—All fluorescence measurements were done at 20 °C with a scan rate of 200 nm/min using the Jasco FP-6300 fluorimeter with the excitation and emission slit widths set at 5 and 10 nm, respectively. The emission spectrum was scanned from 300 to 500 nm with an average of three scans and all spectra corrected for buffer. The nature of the intermediate at the active site of hGST A3-3 was probed using an excitation wavelength of 292 nm in 25 mM sodium phosphate buffer at pH 8 and pH 11 in a total volume of 300 μl with 1% methanol. The equilenin and protein concentrations used were 3 and 9 μM, respectively. The dissociation constant for the binding of equilenin to hGST A3-3 was determined by fluorescence titration of 3 μM equilenin with varying enzyme concentrations ranging between 1 and 15 μM in 25 mM sodium phosphate buffer, pH 8, with 1% methanol. The dependent variable was the emission of free equilenin measured at 363 nm.

Absorbance Measurements with 19-Nortestosterone—Spectral measurements were made in quartz cuvettes with a 1-cm light path. A concentration of 33 μM of 19-nortestosterone with 19.6 μM enzyme was used. The spectrum of the ketosteroid was measured against a 25 mM sodium phosphate buffer blank in 1% methanol. The spectrum of the mixture of ligand and enzyme was measured against a blank containing the enzyme at 19.6 μM with the same buffer composition.

Detection of the Dienolate Intermediate—Zeng and Pollack (13) determined the maximum absorbance wavelength for the externally generated dienolate intermediate to be 238 nm. The UV-visible spectroscopic detection of the dienolate intermediate was followed at 238 nm in 25 mM sodium phosphate buffer at 20 °C and pH 8.0. A total concentration of 10 μM was used for the substrate with 1 μM enzyme concentration.

Solvent Isotope Effects with Δ^5-AD—Steady-state kinetic parameters at 238 and 248 nm were obtained in both D_2O and H_2O in 25 mM phosphate buffer at 20 °C (using potassium deuterium phosphate for D_2O with a pD of 8.0).

The concentrations of substrate were varied from 0.5 to 100 μM. The data were fitted to the Michaelis-Menten equation using SigmaPlot v11 (Systat Software, Inc.). The activity of hGST A3-3 toward Δ^5-AD for the isomerization reaction at 248 nm was determined with a molar extinction coefficient of 16,300 M^{-1} cm^{-1} for Δ^4-AD (8), and the molar extinction coefficient for the formation of the dienolate intermediate was 13,800 M^{-1} cm^{-1} (13). All measurements were done per enzyme subunit with 2 mM GSH at pH 8.

Determination of the Activation Energy—Isomerase activity was recorded from 15 to 40 °C in a thermostatted Varian Cary UV-visible spectrophotometer with a Cary dual cell Peltier accessory. Steady-state kinetic parameters were obtained at 248 and 238 nm with three replicate measures collected for each temperature. The activation energy was determined as described by Tian *et al.* (14) by using the Arrhenius equation ($\ln k = \ln A - E_a/RT$), where k is the rate constant (catalytic turnover), R is the molar gas constant, T is the temperature in degrees Kelvin, E_a is the activation energy, ln is the natural logarithm, and A is the pre-exponential factor. Linear plots of $\ln k$ *versus* $1/T$ yield a slope of $-E_a/R$ from which E_a can be obtained directly. The relationship between the Arrhenius equation and the Eyring transition state equation, k_BT/h exp $(-\Delta G^{\ddagger}/RT)$, yields $\Delta H^{\ddagger} = E_a - RT$, where k_B is the Boltzmann constant, h is the Plank constant, $\Delta G^{\ddagger}$ is the Gibbs free energy of activation, and $\Delta H^{\ddagger}$ is the enthalpy of activation.

RESULTS

The pK_a Value of GSH upon Binding—The binding of the cofactor GSH to hGST A3-3 results in a reduction of the thiol pK_a from the solution value of 9.1 to 6.3 in the active site (Fig. 2). Previous studies on hGST A1-1, a variant of hGST A3-3, indicate a similar reduction for both the isomerization reaction (15) and the typical conjugation reaction (16), equivalent to a reduction in ΔG^0 of 3.8 kcal/mol ($\Delta G^0 = 2.303\ RT\Delta pK_a$).

The Nature of the Intermediate at the Active Site of hGST A3-3—At pH 8.0, free equilenin displays a λ_{max} of 362 nm with a resulting red shift at pH 11 to 425 nm (Fig. 3*A*). The ionization of the aromatic phenol results in the release of electrons previously held in the O–H σ bond, thereby increasing the number of nonbonding electrons capable of making the $n \rightarrow \pi^*$ electronic transition. In the presence of hGST A3-3, the fluorescence emission spectrum resembles the protonated state with a

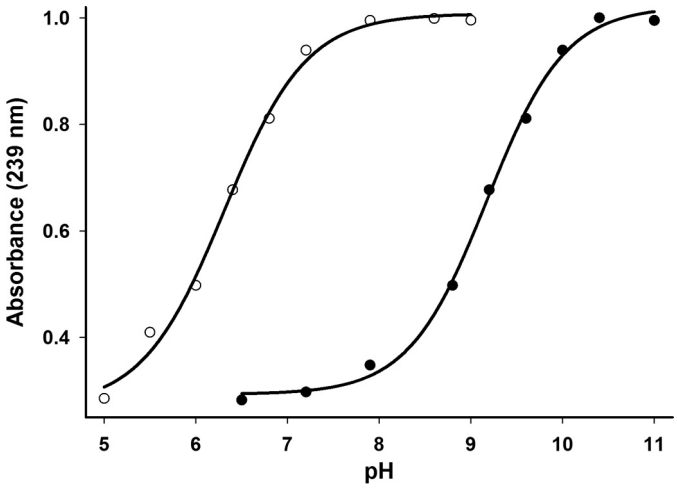

FIGURE 2. **The deprotonation of GSH expressed as a function of pH in the presence and absence of hGST A3-3.** Nonlinear regression analysis of the data yielded a pK_a value of 9.17 ± 0.04 for free GSH (●) and a pK_a value of 6.31 ± 0.07 for the active site-bound GSH (○).

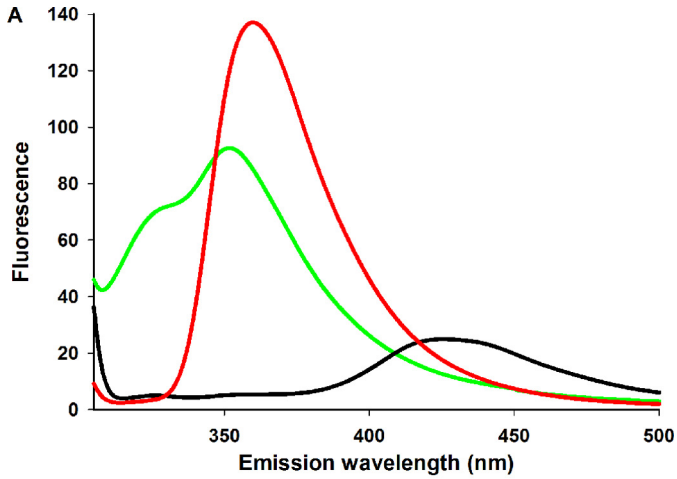

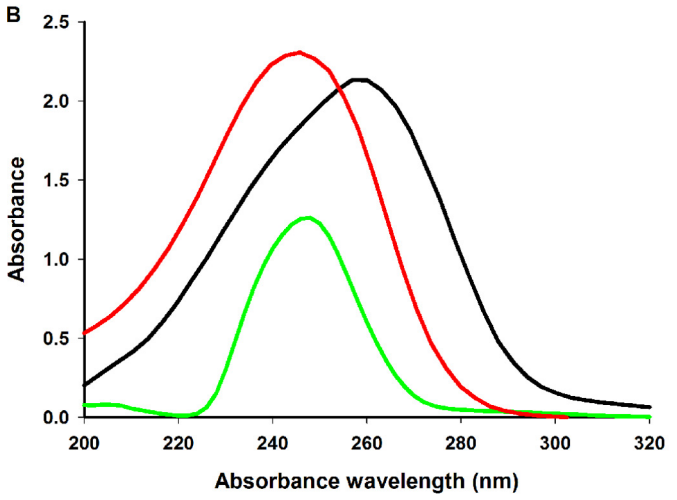

FIGURE 3. *A*, fluorescence emission spectra of equilenin as an indicator of the intermediate ionization state at the active site. Free equilenin (3.8 μM) is observed at pH 8.0 (*red*) and pH 11.0 (*black*) and in the presence of 9 μM enzyme (*green*). Equilenin was dissolved in 1% methanol, and excitation was set at 292 nm. *B*, the absorbance spectra of 19-nortestosterone (36.6 μM) observed in solution at pH 8.0 (*red*), in 10 M HCl (*black*), and in the presence of 19 μM enzyme (*green*).

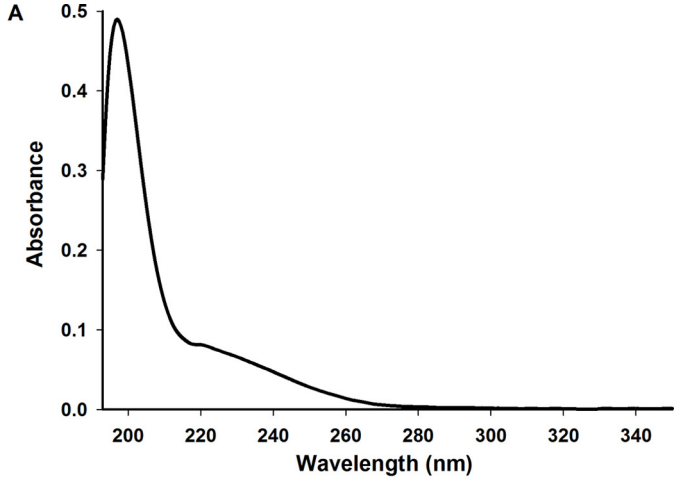

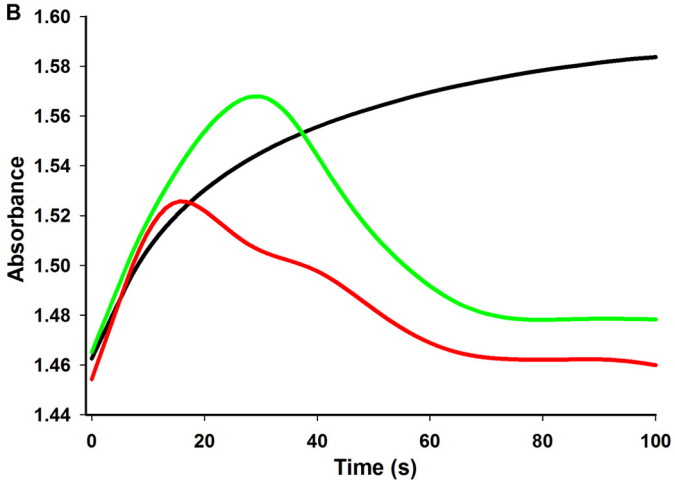

FIGURE 4. *A*, the absorbance spectrum of 150 μM Δ^5-AD in methanol. The isolated ethylenic bond absorbs maximally at 200 nm. *B*, the reaction progress curves of Δ^5-AD followed at 238 nm (*green*), 256 nm (*red*), and 248 nm (*black*).The reactions were done with 1 μM enzyme and 9 μM substrate in 25 mM sodium phosphate, pH 8.0, at 20 °C.

slight shift to 350 nm (Fig. 3*A*). The α,β-unsaturated ketosteroid 19-nortestosterone has a principle absorption maximum at 248 nm in water. A 10-nm shift is observed when the enone chromophore is exposed to 10 M HCl. In the presence of enzyme, the shift is not observed and the absorption maximum remains at 248 nm with a reduction in the concentration of free ligand (Fig. 3*B*).

UV-visible Detection of the Intermediate—The substrate Δ^5-AD displays a λ_{max} of 200 nm because of the isolated double bond (Fig. 4*A*). The principle chromophore at 238 nm however is the conjugated heteroannular diene that is characteristic of the intermediate. Ionization to the enolate frees the O–H-bonding electrons, which make the $n \rightarrow \pi^*$ transition. This transition shifts λ_{max} to 256 nm with a corresponding hyperchromic shift from 13,800 M^{-1} cm^{-1} to 15,000 M^{-1} cm^{-1} (17). The enzymatic conversion of Δ^5-AD was followed at 238, 256, and 248 nm (Fig. 4*B*). The reaction at 248 nm for Δ^5-AD follows product formation, with the chromophoric region being the conjugated α,β-3-ketone isomer. Therefore the reaction does not show a decrease in absorbance, whereas the two progress curves at 238 and 256 nm produce an initial rise in the absor-

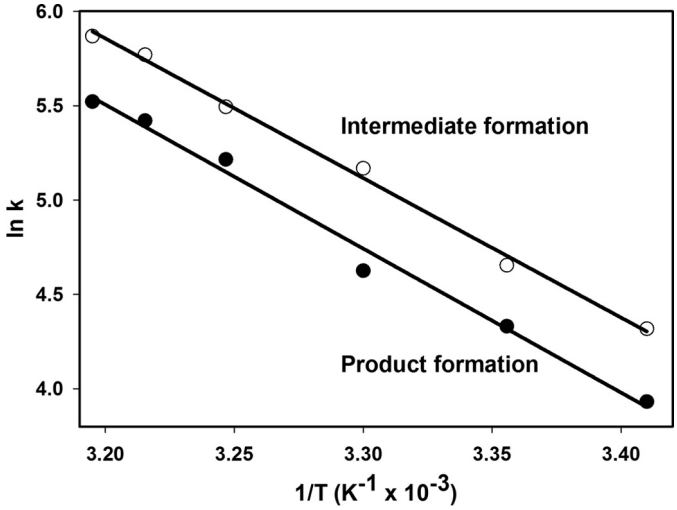

FIGURE 5. The Arrhenius plots for the formation of product (Δ^4-AD) followed at 248 nm yielded an E_a value of 13. 8 ± 0.5 kcal/mol (●) and the formation of the conjugated heteroannular diene intermediate followed at 238 nm yielded an E_a value of 12.9 ± 0.4 kcal/mol (○).

bance followed by a gradual decay corresponding to a decrease in intermediate concentrations.

The Activation Energy of Reaction—The Arrhenius plots for the formation of product at 248 nm and intermediate at 238 nm (Fig. 5) show that the data are linear within the temperature range specified in the experimental procedures. The activation energy at 248 nm is 13.8 kcal/mol and at 238 nm is 12.9 kcal/mol.

Solvent Isotope Effects with Δ^5-AD—Experiments were conducted in which the concentration of Δ^5-AD was varied in H_2O and D_2O, and the initial rates data were fit to Equation 1 describing a random sequential mechanism that is characteristic of GSTs (15).

$$v = \frac{V[A][B]}{K_m^B K_s^A + K_m^B[A] + K_m^A[B] + [A][B]} \quad \text{(Eq. 1)}$$

Steady-state kinetic parameters obtained from the fits are shown in Table 1, where K_s^A is the dissociation constant for the nonvaried substrate and K_m^A and K_m^B are the Michaelis constants for the substrates (18).

The Binding Constant of Equilenin for hGST A3-3—Equilenin was the nonvaried ligand concentration, whereas the hGST A3-3 concentrations ranged from 1 to 15 μM. This unconventional approach of obtaining K_D with a constant ligand concentration and increasing concentrations of enzyme was used because free equilenin is the fluorogenic species. To avoid a protein contribution to the signal, the excitation wavelength used was 325 nm corresponding to the signal produced only by free equilenin (Fig. 6*A*). This information was used to obtain the K_D by monitoring the decrease in fluorescence intensity. The data were fit to a three-parameter hyperbolic decay curve (Equation 2), where F is the fluorescence intensity, $F\infty$ is the extrapolated intensity to infinite enzyme concentrations, F_o is the intensity in the absence of enzyme, $[E_T]$ is the total enzyme concentration, and $[L_T]$ is the total ligand (equilenin) concentration (Fig. 6*B*). The K_D value calculated was 3.93 ± 0.53 μM,

TABLE 1

Solvent isotope exchange with Δ^5–AD at 238 and 248 nm

The enzyme activity with Δ^5-AD was measured with 2 mM saturating GSH in H_2O and D_2O at 20 °C. H_2O refers to 25 mM protiated phosphate buffer at pH 8.0, and D_2O refers to deuterated phosphate buffer at pD 8.0.

Wavelength (nm)	k_{cat}	K_m	k_{cat}/K_m	K_s	Specific activity
	s^{-1}	μM	$mM^{-1}\ s^{-1}$	μM	$\mu mol\ mg^{-1}\ min^{-1}$
H_2O (238)	75 ± 4	20.2 ± 3.4	1700 ± 150		
D_2O (238)	70.4 ± 3.5	19.7 ± 2.3	1400 ± 155		
D_2O (248)	41.7 ± 4.2	13.2 ± 1.8	1100 ± 100		51 ± 5
H_2O (248)	51 ± 3	22.5 ± 4.3	2000 ± 198	9.3 ± 2.2[a]	76 ± 2
GSH (248)		130 ± 21	370 ± 60	50 ± 10[b]	

[a] Determined with a constant Δ^5-AD concentration of 200 μM and varying the GSH concentration.

[b] Determined with a constant GSH concentration of 2 mM and varying the Δ^5-AD concentration.

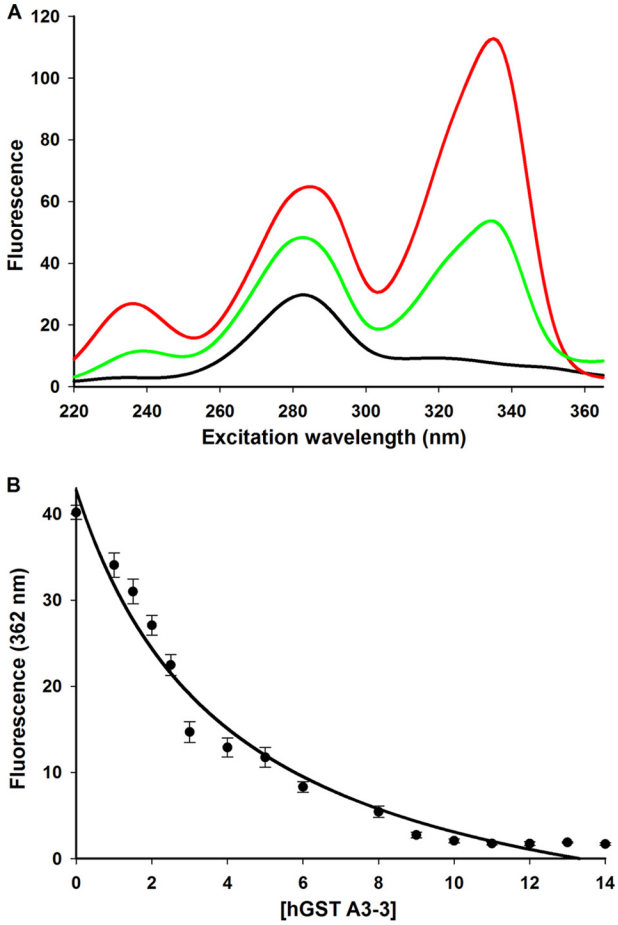

FIGURE 6. **The fluorescence excitation (*A*) of equilenin and hGST A3-3 used to obtain a binding curve (*B*).** The fluorescence data in *A* were collected for free equilenin (*red*), equilenin in the presence of hGST A3-3 (*green*), and free hGST A3-3 (*black*). A quenching effect is observed in the excitation spectra. The emission wavelength was set at 400 nm for *A*, and excitation was set at 325 nm for *B*. The data were fit to a three-parameter hyperbolic decay curve yielding a K_D value of 3.93 ± 0.53 μM. Measurements were done in 1% methanol at pH 8.0 with 3 μM equilenin.

$$F = F_\infty + \frac{\{(F_o - F) - k[E_T]\}K_D}{[E_T]} \quad \text{(Eq. 2)}$$

where $k = F_o - F\infty/[L_T]$.

DISCUSSION

Energetics of Proton Abstraction Reactions—Carbon acids (C–H bonds adjacent to a carbonyl or carboxylic acid func-

tional group) are generally very weak acids with pK_a values of the α-protons in the range of 12 to 32 (19). At the active site, the general base catalysts are not sufficiently basic, with pK_a values usually $\leq$7 (20). The large pK_a difference between the substrate and the active site base poses a thermodynamic challenge. To overcome this challenge, enzymes have evolved structural features capable of reducing this thermodynamic contribution to the activation energy.

The binding of the cofactor GSH to hGST A3-3 results in a reduction in the thiol pK_a from 9.17 to 6.31. Consequently at pH 8.0 the cofactor exists in its ionized state. The crystal structure of the ternary complex of hGST A3-3, GSH and the product Δ^4-AD reveals that the thiol group of GSH is 3.7 Å from the carbon 4 atom of Δ^4- AD (11), an ideal distance for proton abstraction. The consensus has been that the ionized thiol plays a role similar to Asp-38 in the KSI-catalyzed reaction, abstracting a proton from the carbon 4 of Δ^5-AD.

The use of chromophoric steroids as a tool to probe the nature of intermediates in ketosteroid isomerization was first reported by Wang *et al.* (21). Fluorescence emission data were used to monitor the ionization state of the phenolic analog intermediate equilenin (Fig. 3*A*). The breaking of the O–H bond in the aromatic phenol increases the number of nonbonding electrons capable of making the $n \rightarrow \pi^*$ electronic transition. This transition requires less energy, and as such a bathochromic shift is observed at pH 11 (21–24). The results indicate that in the presence of hGST A3-3 the emission spectrum resembles that of the un-ionized equilenin. In contrast, the binding of equilenin to KSI results in a spectrum that resembles the ionized state (25). The enone chromopore is responsible for the UV spectral behavior of the ketosteroid competitive inhibitor 19-nortestosterone (Fig. 3*B*). A 10-nm transition of the absorption maximum of this compound from 248 to 258 nm is attributed to enolization, protonation, or strong hydrogen bonding, mimicking its own behavior in strong acid (21, 23, 25, 26).

Our results shown in Fig. 3 indicate that these shifts in wavelength do not occur in the enzyme active site. As hGST A3-3 binds its substrate in the hydrophobic H-site, the generation of charge that accompanies dienolate formation is unfavorable in the solvent-inaccessible hydrophobic environment without the formation of strong directional hydrogen-bonding interactions (26). Our results support the current structural data and show no evidence of such directional hydrogen bonds; consequently the existence of the dienolate would either be a transient feature in a thermodynamically driven pathway, where the final product is more stable, or it would be a nonexistent feature if the end product was merely its own formation. In the KSI mechanism, Asp-99 and Tyr-14 stabilize the intermediate by hydrogen bonding, the D99A mutation decreases the k_{cat} value by $10^{3.7}$ (27), and the Y14F mutation decreases the k_{cat} value by $10^{4.7}$ (23). These mutations result in catalytic turnovers that compare well with the observed turnover value for hGST A3-3, suggesting that this enzyme may be devoid of such strong hydrogen-bonding interactions. The thiolate of GSH acts as the base catalyst but without an equivalent acidic residue at the C3 oxygen, a general, concerted, acid-base catalysis that enhances intermediate stabilization in the enolization step would not occur.

To verify the transient existence of the dienolate in a thermodynamically favored reaction, the isomerization of Δ^5-AD was followed at 238 nm. This wavelength detects the formation of the conjugated heteroannular diene intermediate. The substrate Δ^5-AD possesses an isolated double bond (unconjugated) for which the apparent λ_{max} is calculated to be 203 nm, with an extinction coefficient no greater than 4000 M^{-1} cm^{-1} (28). The principle absorption wavelength for Δ^5-AD is λ_{max} = 200 nm, with a calculated extinction coefficient of 3800 M^{-1} cm^{-1} (Fig. 4*A*). However, the effect of conjugation results in a bathochromic and hyperchromic displacement of the principle absorption band resulting in an increased extinction coefficient of 13,800 M^{-1} cm^{-1} (λ_{max} = 238 nm). The product, Δ^4-AD, has an α,β-ethylenic center conjugated with the 3-keto group. The effect of alkyl substituents on the double bond chromophore is a bathochromic displacement. This displacement, however, does not occur with the same regularity among the three chromophoric regions that constitute the three species in the catalytic pathway: (i) the isolated double bond in the substrate Δ^5-AD, (ii) the conjugated diene in the intermediate species, and (iii) the α,β-unsaturated ketone of the product Δ^4-AD (29). There is a 30–40-nm shift in wavelength in moving from an isolated double bond to a conjugated diene and an additional 11–15-nm wavelength shift from the conjugated diene to the α,β-unsaturated ketone (28–30), with such changes attributed to bond strain and alterations in the planarity of the resonating system. The results in Fig. 4*B* indicate that such transient intermediate species, for which the only form of stabilization is electron delocalization through a conjugate system, do exist. Furthermore, the existence of the transient dienolate intermediate verifies its importance in the catalytic pathway. The intermediate species accumulates and gradually decays because of its transience in the isomerization process. The effect of the carbonyl group at carbon 3 on the rate of isomerization becomes significant only in the presence of strong hydrogen bonds. In the absence of such strong bonds, conjugation becomes the major stabilizing force with only a minimal contribution from the electronegative oxygen atom. The inability of hGST to offer further stability by hydrogen bonding (as is the case with the KSI-catalyzed reaction) means that the intermediate concentrations are not sufficient to account for a turnover similar to that of KSI.

The Marcus Formalism—In proton and electron transfer reactions, rather than considering the activation energy as a single measurable quantity, the Marcus formalism (12, 31–34) divides the activation energy ($\Delta G^{\dagger}$) into two components, (i) the thermodynamic free energy barrier (ΔG^0) and (ii) the intrinsic kinetic barrier ($\Delta G^{\dagger}_{int}$), as shown in Equation 3,

$$\Delta G^{\dagger} = \Delta G^{\dagger}_{int} + \frac{\Delta G^0}{2} + \frac{(\Delta G^0)^2}{16\Delta G^{\dagger}_{int}} \qquad \text{(Eq. 3)}$$

where $\Delta G^{\dagger}_{int}$ is the activation energy barrier in the absence of any thermodynamic contributions (*i.e.* when $\Delta G^0 = 0$). In proton transfer reactions, ΔG^0 is a function of ΔpK_a and is given by $\Delta G^0 = 2.303\ RT\Delta pK_a$ (ΔpK_a is the difference in the pK_a values

between the proton donor and acceptor) (35). The position of the transition state occurs at the maximum value of Equation 3 and is given by Equation 4, which equals the Brønsted coefficient, β_c.

$$x^{\dagger} = \beta_c = 0.5 + \frac{\Delta G^0}{8\Delta G^{\dagger}_{int}} \quad \text{(Eq. 4)}$$

In the hGST A3-3-catalyzed reaction, the k_{cat} obtained for the isomerization of Δ^5-AD translates into an activation energy of 13.8 kcal/mol from the Arrhenius plots in Fig. 5 and a calculated $\Delta G^{\dagger} = 14.8$ kcal/mol (according to the Eyring transition state equation). The hGST-catalyzed isomerization reaction has been found to follow a random sequential mechanism (15). If the model of Reaction 1 (E = enzyme, G = glutathione, S = Δ^5-AD, I = intermediate, and P = product) for a random sequential mechanism is used (where 2 mM GSH and enzyme are incubated first to prevent initial random binding), then the k_{cat} is given by Equation 5 (36).

$$EG + S \underset{k_2}{\overset{k_1}{\rightleftharpoons}} EGS \underset{k_4}{\overset{k_3}{\rightleftharpoons}} EGI \underset{k_6}{\overset{k_5}{\rightleftharpoons}} EGP \left\{ \begin{array}{l} \underset{k_8}{\overset{k_7}{\rightleftharpoons}} EP \underset{k_{10}}{\overset{k_9}{\rightleftharpoons}} E + P \\ \underset{k_{12}}{\overset{k_{11}}{\rightleftharpoons}} EG \underset{k_{14}}{\overset{k_{13}}{\rightleftharpoons}} E + G \end{array} \right.$$

REACTION 1

$$\frac{1}{k_{cat}} = \frac{1}{k'_3} + \frac{1}{k'_5} + \frac{1}{k'_{7,11}} \quad \text{(Eq. 5)}$$

where k'_3, k'_5, and $k'_{7,11}$ are net rate constants, with $k'_{7,11} = k_9k_{13}(k_{11} + k_7)/k_9k_{13} + k_9k_{11} + k_7k_{13}$. The value of the apparent second order rate constant indicates that the hGST A3-3-catalyzed reaction is not diffusion-controlled, despite the high catalytic efficiency. This coupled with the fact that the product, Δ^4-AD (with a K_i of 25 μM), has the same affinity as the substrate (5) means that the net rate constants for dissociation are large (non-limiting). Thus Equation 5 approximates to Equation 6.

$$\frac{1}{k_{cat}} \approx \frac{1}{k_3'} + \frac{1}{k_5'} \quad \text{(Eq. 6)}$$

Given that $k_6 \ll (k_7 + k_{11})$,

$$k_{cat} \approx \frac{k_3k_5}{k_4 + k_5} \quad \text{(Eq. 7)}$$

The microscopic rate constants reveal that the rate-limiting steps are the chemical steps: proton abstraction from carbon 4, proton transfer to carbon 6, and proton transfer back to carbon 4 (Equation 7). The reaction at 238 nm is best described by Reaction 2. The reverse reaction from *EGI to EGS* (k_4) is assumed to be zero as initial rates are considered.

$$EG + S \underset{k_2}{\overset{k_1}{\rightleftharpoons}} EGS \overset{k_3}{\rightleftharpoons} EGI$$

REACTION 2

The results shown in Table 1 reveal that in H_2O, the k_{cat} for the overall reaction followed at 248 nm is comparable with the k_{cat} value for the reaction followed at 238 nm. Because this value represents k_3, the proton abstraction step is rate-limiting. This allows us to use the macroscopic k_{cat} value as an approximation to the microscopic rate constant k_3 of the proton abstraction in the Marcus equation. In assessing the contribution of the carbon 6 proton transfer step to the overall rate, solvent isotope effects are employed. The H/D isotopic exchange between solvent and substrate occurs at the intermediate during the proton transfer step. In both reactions followed at 238 and 248 nm, $({}^{H}k_{cat})/({}^{D}k_{cat}) \approx 1$, suggesting that the carbon 6 proton transfer step is nonlimiting, whereas the carbon 4 proton abstraction step is independent of H/D exchange with solvent.

This analysis however overlooks the possibility of protonation back to carbon 4 in the reverse reaction. The rate of carbon 4 protonation would be given by Equation 8,

$$k_r = \frac{k_2k_4}{k_2 + k_3} \quad \text{(Eq. 8)}$$

where k_r is the net rate constant for reverse protonation at carbon 4; because the diffusion steps are rapid ($k_2 \ll k_3$), the value of $k_r \approx k_4$. The internal equilibrium constant between substrate and intermediate has been found ($K_{int} = 0.3$) (37). This internal equilibrium constant indicates that the relative energies of the substrate and intermediate are similar. Because the free energy of reaction favors product formation ($K_{eq} = 2400$) (17), the energy barrier for carbon 4 protonation back to reactant is much larger than the carbon 6 protonation for the forward reaction. Therefore the k_{cat} values for the forward reactions are minimally affected by the possible carbon 4 protonation.

If the pK_a of Δ^5-AD remains invariant upon binding the H-site, then the thermodynamic energy required for proton abstraction is $\Delta G^0 = 9$ kcal/mol (pK_a of bound GSH is 6.31). The value obtained for the intrinsic kinetic barrier from Equation 2 is $\Delta G^{\dagger}_{int} = 10$ kcal/mol. Hawkinson *et al.* (37) calculated the intrinsic barrier for proton transfer from Δ^5-AD in solution to be ($\Delta G^{\dagger}_{int} = 13$ kcal/mol. This value was obtained by estimating the Brønsted β_c value of oxygen bases from tertiary amine and oxygen bases involved in the isomerization of 3-cyclohexanone. A β_c value of 0.6 was obtained, representative of the acetate oxygen base used to catalyze the solution reaction. The actual β value for the acetate ion-catalyzed ketonization is 0.54 (38), verifying the accuracy of the Hawkinson approximation. Due credence must however encompass the role of the thiol as the base. Oxidized glutathione and similar thiols have β_c values ranging between 0.5 and 0.55 (39, 40); because the basicity of thiols is expected to be greater than resonance-stabilized oxygen bases such as acetates, the upper limit value of this range was used, and the Hawkinson approximation was still upheld. The strategy of hGST A3-3 appears in part to reduce the intrinsic kinetic barrier by 3 kcal/mol. The Brønsted coefficient describing the position of the transition state is $\beta_c = 0.6$, a value that indicates a nearly symmetrical transition state.

Revised Mechanism—The hGST A3-3 reaction pathway is initiated by proton abstraction at carbon 4 of Δ^5-AD (Fig. 7). During proton abstraction, a negative charge develops at the

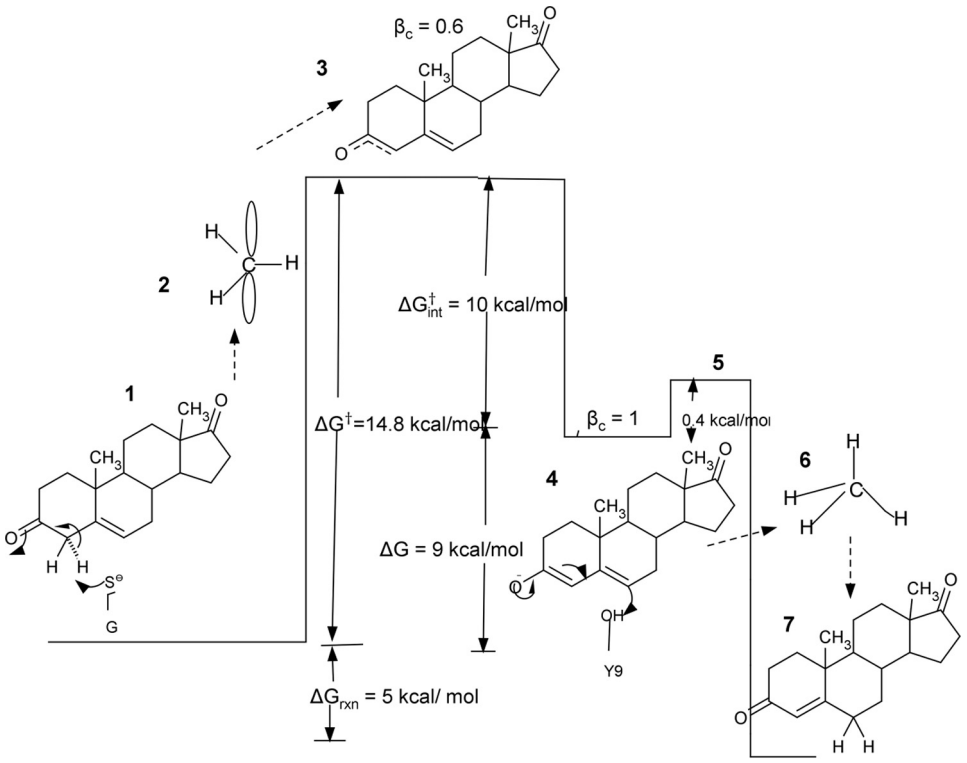

FIGURE 7. **The proposed reaction pathway for the isomerization of Δ^5-AD by hGST A3-3, were the *steps* are numbered *1–7* and the thermodynamic parameters are calculated per enzyme subunit.** At *step 1*, GSH abstracts the carbon 4 proton; at *step 2* a change in hybridization at carbon 4 to a higher energy *p*-orbital; at *step 3*, a transition state occurs that is nearly symmetrical but slightly favors the intermediate. At *step 4* the structural realignments have advanced since the transition state, and the high energy *p*-orbital electrons are stabilized by the now fully developed conjugate system. At *step 5* the transfer of a proton to carbon 6 is kinetically insignificant, resulting in an enforced concerted mechanism, and at *step 6* a transfer of electrons from the *p*-orbital to the lower energy sp3 orbital resulting in *step 7*.

site of bond cleavage, and the carbon 4 carbon transits from sp3 hybridization to sp2. This transition is energetically unfavorable because the electrons from the lower energy sp3 orbital are transferred to the vacant *p*-orbital of higher energy. At the energy maxima, the transition state is nearly symmetrical but slightly favors the intermediate, as indicated by the Brønsted coefficient ($\beta_c = 0.6$). As structural rearrangement progresses, electrons in the higher energy *p*-orbital are stabilized by the O3-C3-C4-C5-C6 conjugate system. Charge development has the effect of realigning the dipoles of active site water molecules, thereby producing a negative entropic contribution due to solvent ordering (33). The intrinsic kinetic barrier $\Delta G^{\dagger}_{\mathrm{int}}$ refers to the energy that has to be overcome in making such an unfavorable electronic configuration as well as the negative entropic contribution associated with solvent ordering (41). Conjugation alone has a minimal contribution to the overall stability of the intermediate. The strategy of hGST A3-3 is to lower $\Delta G^{\dagger}_{\mathrm{int}}$ with a value of 13 kcal/mol in solution to $\Delta G^{\dagger}_{\mathrm{int}} = 10$ kcal/mol at the active site. The enzyme utilizes an alternative reaction pathway that alters the cofactor pK_a, thereby contributing 3.8 kcal/mol to the reaction. Although the altered pK_a of GSH contributes to the ΔG^0 favorably, the enzyme has no structural features such as amino acids capable of forming hydrogen bonds and is thus incapable of effectively dealing with the developing charge. As the free energy of reaction favors product formation ($K_{\mathrm{eq}} = 2400$) and the realization that the chemical steps are rate-limiting, proton transfer to carbon 6 (resulting in product) is therefore a fast step. Solvent isotope exchange reveals that this energetic barrier is 0.4 kcal/mol. As the kinetics studies follow product (and intermediate) formation, this energetic barrier does not include the regeneration of the protonated Tyr-9 but merely the transfer of a proton to carbon 6. We propose that hGST A3-3 lowers the $\Delta G^{\dagger}_{\mathrm{int}}$ by accelerating the rate of proton transfer to carbon 6, making this the fast step. The rapid transfer of the proton minimizes the extent of charge imbalance at the transition state and intermediate, ultimately reducing the negative entropic contribution associated with solvent ordering at the active site. because $\Delta G^{\dagger}_{\mathrm{int}} = \Delta H^{\dagger}_{\mathrm{int}} + T\Delta S^{\dagger}_{\mathrm{int}}$ (33), a reduction in the loss of entropy contributes to lowering the activation energy. The K_D value of 3.93 μM for equilenin (Fig. 6*B*) indicates that the protonated form of the intermediate has an affinity for binding similar to that of the substrate (as indicated by the K_S value). Although we could not obtain the K_D of ionized equilenin without compromising enzyme structure, a comparison of the K_D values of hGST A3-3 and KSI provided further insight. The K_D of equilenin for KSI is 1 μM (37), a value similar to that of hGST A3-3. However, the rate of the KSI-catalyzed reaction is greater than that of hGST A3-3 by 3 orders of magnitude, suggesting greater dienolate intermediate concentrations for the KSI reaction. Therefore, the critical difference is charge stabilization. A computational analysis using a hybrid quantum mechanics/molecular mechanics approach is in agreement with this mechanism, which proceeds via an intermediate (42). The reported thermodynamic parameters of

this computational study are however nearly 2-fold greater than our reported values and may represent the dimeric protein instead of subunit values. Recently, Ramos and co-workers (43) have reconstructed the catalytic pathway by resorting to density functional theory, and their findings show that water molecules are neither necessary nor responsible for stabilizing the intermediate. They however attribute this stability to strong hydrogen bonds formed between the GSH-glycine main chain and the C3 oxygen (43). This is supported by kinetic studies in which the K_m value increases from 45 to 310 μM in the absence of GSH, suggesting a reduced affinity for Δ^5-AD due to the absence of this hydrogen bond. The use of K_m as an approximate measure for binding affinity becomes problematic with increased kinetic complexity. This value becomes a composite function of many microscopic rate constants, and its contribution to the observed value may be significant depending on the dominant enzyme-bound state. Nonetheless, if this approximation is accepted and further concession is made that this binding energy is realized most strongly at the transition-intermediate stages, the increase in the K_m value from 45 to 310 μM would only account for an energy difference of $\sim$1 kcal/mol, indicating that the contribution of the GSH-glycine main chain hydrogen bond with O3 contributes very little to the kinetic process.

The mechanism shown in Fig. 1, **Scheme I**, postulates the existence of a localized water molecule to stabilize a transient dienolate intermediate at the C3 oxygen similar to the roles of Tyr-14 and Asp-99 in the KSI-catalyzed reaction; however, neither our results nor the currently available structural data support this view. The mechanism shown in Fig. 1, **Scheme II**, proposes a reaction pathway that avoids the formation of the dienolate by placing a transient double bond at the α,β-positions. The mechanism implies perfect synchronization of the bond-breaking and -making process, as anything less would result in an overcommitted β-carbon with five bonds. Although this is within the realm of possibility, charge delocalization has been seen to lag behind proton transfer due to a lag in resonance development in carbon acids (41) and specifically in enzymatic enolization reactions (38). Furthermore electron movement against an electronegativity gradient and a conjugate system that offers stability is unlikely. As the chemical steps are rate-limiting and the K_{eq} favors product formation, the energy barrier to product formation cannot exceed that of the decomposition back to substrate. Because of the instability of the dienolate intermediate, in which only form of stabilization is charge delocalization, the collapse to product, which is strongly favored thermodynamically, may not be activation-limited, making this step kinetically insignificant. We are of the view that reaction proceeds through an enforced, concerted mechanism (44, 45) that results from changes in a stepwise process, where the energy that corresponds well to an intermediate is nearly commensurate with a regular, concerted mechanism.

Acknowledgments—We thank Professor Emeritus Ralph Pollack for valuable and insightful suggestions on certain aspects of the experimental design and Monika Nowakowska for assistance rendered with the thermostated Varian Cary UV-visible spectrophotometer.

REFERENCES

1. Armstrong, R. N. (1997) Structure, catalytic mechanism, and evolution of the glutathione transferases. *Chem. Res. Toxicol.* **10,** 2–18
2. Mannervik, B., and Danielson, U. H. (1988) Glutathione transferase-structure and catalytic activity. *CRC Crit. Rev. Biochem.* **23,** 283–337
3. Dirr, H., Reinemer, P., and Huber, R. (1994) X-ray crystal structures of cytosolic glutathione *S*-transferases. *Eur. J. Biochem.* **220,** 645–661
4. Benson, A. M., and Talalay, P. (1976) Role of reduced glutathione in the Δ(5)-3-kitosteroid isomerase reaction of liver. *Biochem. Biophys. Res. Commun.* **69,** 1073–1079
5. Johansson, A. S., and Mannervik, B. (2001) Human glutathione transferase A3-3, a highly efficient catalyst of double-bond isomerization in the biosynthetic pathway of steroid hormones. *J. Biol. Chem.* **276,** 33061–33065
6. Montgomery, R., Conway, T. W., Spector, A. A., and Chappell, D. (1996) Biochemistry: A Case-oriented Approach, 6th Ed., pp. 587–618, Mosby Year Book, Inc., St. Louis, MO
7. Talalay, P., and Wang, V. S. (1955) Enzymic isomerization of Δ5-3-ketosteroids. *Biochim. Biophys. Acta* **18,** 300–301
8. Benson, A. M., Talalay, P., Keen, J. H., and Jakoby, W. B. (1977) Relationship between the soluble glutathione-dependent Δ5-3-ketosteroid isomerase and the glutathione *S*-transferases of the liver. *Proc. Natl. Acad. Sci. U.S.A.* **74,** 158–162
9. Hawkinson, D. C., Eames, T. C., and Pollack, R. M. (1991) Energetics of 3-oxo-Δ 5-steroid isomerase: source of the catalytic power of the enzyme. *Biochemistry* **30,** 10849–10858
10. Gu, Y., Guo, J., Pal, A., Pan, S. S., Zimniak, P., Singh, S. V., and Ji, X. (2004) Crystal structure of human glutathione *S*-transferase A3-3 and mechanistic implications for its high steroid isomerase activity. *Biochemistry* **43,** 15673–15679
11. Tars, K., Olin, B., and Mannervik, B. (2010) Structural basis for featuring of steroid isomerase activity in α class glutathione transferases. *J. Mol. Biol.* **397,** 332–340
12. Marcus, R. A. (1969) Unusual slopes of free energy plots in kinetics. *J. Am. Chem. Soc.* **91,** 7224–7225
13. Zeng, B., and Pollack, R. M. (1991) Microscopic rate constants for the acetate ion catalyzed isomerization of 5-androstene-3,17-dione to 4-androstene-3,17-dione: a model for steroid isomerase. *J. Am. Chem. Soc.* **113,** 3838–3842
14. Tian, X. Q., Chen, T. C., Matsuoka, L. Y., Wortsman, J., and Holick, M. F. (1993) Kinetic and thermodynamic studies of the conversion of previtamin D3 to vitamin D3 in human skin. *J. Biol. Chem.* **268,** 14888–14892
15. Pettersson, P. L., and Mannervik, B. (2001) The role of glutathione in the isomerization of delta 5-androstene-3,17-dione catalyzed by human glutathione transferase A1-1. *J. Biol. Chem.* **276,** 11698–11704
16. Caccuri, A. M., Antonini, G., Board, P. G., Parker, M. W., Nicotra, M., Lo Bello, M., Federici, G., and Ricci, G. (1999) Proton release on binding of glutathione to alpha, mu, and delta class glutathione transferases. *Biochem. J.* **344,** 419–425
17. Pollack, R. M., Zeng, B., Mack, J. P. G., and Eldin, S. (1989) Determination of the microscopic rate constants for the base-catalyzed conjugation of 5-androstene-3,17-dione. *J. Am. Chem. Soc.* **111,** 6419–6423
18. Cleland, W. W. (1963) The kinetics of enzyme-catalyzed reactions with two or more substrates or products. I. Nomenclature and rate equations. *Biochim. Biophys. Acta* **67,** 104–137
19. Chiang, Y., and Kresge, A. J. (1991) Enols and other reactive species. *Science* **253,** 395–400
20. Gerlt, J. A., Kozarich, J. W., Kenyon, G. L., and Gassman, P. G. (1991) Electrophilic catalysis can explain the unexpected acidity of carbon acids in enzyme-catalyzed reactions. *J. Am. Chem. Soc.* **113,** 9667–9669
21. Wang, S. F., Kawahara, F. S., and Talalay, P. (1963) The mechanism of the Δ5-3-ketosteroid isomerase reaction: absorption and fluorescence spectra of enzyme-steroid complexes. *J. Biol. Chem.* **238,** 576–585
22. Bevins, C. L., Pollack, R. M., Kayser, R. H., and Bounds, P. L. (1986) Detection of a transient enzyme-steroid complex during active-site-directed irreversible inhibition of 3-oxo-Δ 5-steroid isomerase. *Biochemistry* **25,** 5159–5164
23. Kuliopulos, A., Mildvan, A. S., Shortle, D., and Talalay, P. (1989) Kinetic

and ultraviolet spectroscopic studies of active-site mutants of Δ5-3-ketosteroid isomerase. *Biochemistry* **28,** 149–159
24. Eames, T. C., Pollack, R. M., and Steiner, R. F. (1989) Orientation, accessibility, and mobility of equilenin bound to the active site of steroid isomerase. *Biochemistry* **28,** 6269–6275
25. Zeng, B. F., Bounds, P. L., Steiner, R. F., and Pollack, R. M. (1992) Nature of the intermediate in the 3-oxo-Δ 5-steroid isomerase reaction. *Biochemistry* **31,** 1521–1528
26. Zhao, Q., Mildvan, A. S., and Talalay, P. (1995) Enzymic and nonenzymic polarizations of. α,β-unsaturated ketosteroids and phenolic steroids: implications for the roles of hydrogen bonding in the catalytic mechanism of Δ 5-3-ketosteroid isomerase. *Biochemistry* **34,** 426–434
27. Wu, Z. R., Ebrahimian, S., Zawrotny, M. E., Thornburg, L. D., Perez-Alvarado, G.C., Brothers, P., Pollack, R. M., and Summers, M. F. (1997) Solution structure of 3-oxo-Δ5-steroid isomerase. *Science* **276,** 415–418
28. Bladon, P., Henbest, H. B., and Wood, G. W. (1952) Studies in the sterol group. Part LV. Ultra-violet absorption spectra of ethylenic centres. *J. Chem. Soc.* **517,** 2737–2744
29. Woodward, R. B. (1941) Structure and the absorption spectra of α,β-unsaturated ketones. *J. Am. Chem. Soc.* **63,** 1123–1126
30. Dorfman, L. (1953) Ultraviolet absorption of steroids. *Chem. Rev.* **53,** 47–144
31. Cohen, A. O., and Marcus, R. A. (1968) Slope of free energy plots in chemical kinetics. *J. Phys. Chem.* **72,** 4249–4256
32. Albery, W. J. (1980) The application of the Marcus relation to reactions in solution. *Annu. Rev. Phys. Chem.* **31,** 227–263
33. Gerlt, J. A., and Gassman, P. G. (1993) Understanding the rates of certain enzyme-catalyzed reactions: proton abstraction from carbon acids, acyl transfer reactions, and displacement reactions of phosphodiesters. *Biochemistry* **32,** 11943–11952
34. Marcus, R. A. (2006) Enzymatic catalysis and transfers in solution. I. Theory and computations, a unified view. *J. Chem. Phys.* **125,** 194504
35. Gerlt, J. A., and Gassman, P. G. (1992) Understanding enzyme-catalyzed proton abstraction from carbon acids: details of stepwise mechanisms for β-elimination reactions. *J. Am. Chem. Soc.* **114,** 5928–5934
36. Cleland, W. W. (1975) Partition analysis and concept of net rate constants as tools in enzyme kinetics. *Biochemistry* **14,** 3220–3224
37. Hawkinson, D. C., Pollack, R. M., and Ambulos, N. P., Jr. (1994) Evaluation of the internal equilibrium constant for 3-oxoΔ 5-steroid isomerase using the D38E and D38N mutants: the energetic basis for catalysis. *Biochemistry* **33,** 12172–12183
38. Yao, X., Gold, M. A., and Pollack, R. M. (1999) Transition state imbalance in proton transfer from phenyl ring-substituted 2-tetralones to acetate ion. *J. Am. Chem. Soc.* **121,** 6220–6225
39. Szajewski, R. P., and Whitesides, G. M. (1980) Rate constants and equilibrium constants for thiol-disulfide interchange reactions involving oxidized glutathione. *J. Am. Chem. Soc.* **102,** 2011–2026
40. Dalby, K. N., and Jencks, W. P. (1997) General acid catalysis of the reversible addition of thiolate anions to cyanamide. *J. Chem. Soc. Perkin Trans.* **2,** 1555–1564
41. Bernasconi, C. F. (1992) The principle of nonperfect synchronization: more than a qualitative concept? *Acc. Chem. Res.* **25,** 9–16
42. Calvaresi, M., Stenta, M., Garavelli, M., Altoé, P., and Bottoni, A. (2012) Computational evidence for the catalytic mechanism of human glutathione *S*-transferase A3-3: a QM/MM investigation. *ACS Catal.* **2,** 280–286
43. Dourado, D. F., Fernandes, P. A., Mannervik, B., and Ramos, M. J. (2014) Isomerization of Δ5-androstene-3,17-dione into Δ4-androstene-3,17-dione catalyzed by human GST A3-3: a computational study identifies a dual role for glutathione. *J. Phys. Chem. A* **118,** 5790–5800
44. Williams, A. (1994) The diagnosis of concerted organic mechanisms. *Chem. Soc. Rev.* **23,** 93–100
45. Jencks, W. P. (1981) Ingold lecture: how does a reaction choose its mechanism? *Chem. Soc. Rev.* **10,** 345–375